

Award Accounts

The Chemical Society of Japan Award for Creative Work for 2005

Photochemistry and Photo-Induced Ultrafast Dynamics at Metal Surfaces

Yoshiyasu Matsumoto

National Institutes of Natural Sciences, Institute for Molecular Science, Okazaki 444-8585

Department of Photoscience, School of Advanced Sciences, The Graduate University for Advanced Studies (Sokendai), Hayama 240-0193

Received August 31, 2006; E-mail: matsumoto@ims.ac.jp

This account describes excitation mechanisms and ultrafast nuclear dynamics at metal surfaces induced upon photon irradiation. After reviewing possible excitation mechanisms for photochemistry of adsorbates on metal surfaces, we discuss the ultra-violet photochemistry of saturated hydrocarbons, i.e., methane and cyclohexane, on metal surfaces. Although these alkanes in the gas phase do not absorb photons at ≈6 eV, CH bond dissociation takes place upon 6.4-eV photon irradiation on metal surfaces. Hybridization between CH antibonding orbitals of the alkanes and metal bands, forming a new band across the Fermi level, is proposed to be responsible for both the photochemistry and CH vibrational mode softening. Since electronic relaxation at metal surfaces takes place very rapidly, most of excited adsorbates do not proceed to dissociation and/or desorption, but rather they are vibrationally excited. To probe photo-induced nuclear motions in real time, we developed femtosecond (fs) time-resolved second harmonic generation spectroscopy on metal surfaces. This method was used to explore the dynamics of photo-excited coherent vibration at Pt(111) surfaces covered with alkali-metal atoms. Irradiation of fs pump-laser pulses induced coherent vibrational motions of the stretching vibration of alkali atoms with respect to the metal surface and the Rayleigh modes of the Pt surface, which manifest themselves in modulations of second harmonic intensity of probe pulses. We also demonstrated that selective excitation of a phonon mode can be achieved by using tailored light pulse trains.

1. Introduction

Photo-induced processes at surfaces have attracted a keen interest from researchers in both fundamental and applied fields. Photo-irradiation at surfaces induces electronic excitation of adsorbates and substrates, leading to various processes including charge transfer between adsorbates and substrates and chemical reactions of adsorbates. Thus, these photo-induced processes provide an excellent opportunity for studying their electronic structures and nuclear dynamics. Moreover, they are very relevant to technologies involving photocatalysts, microelectronics fabrication, optoelectronic devices using organic semiconductors, etc. Therefore, the photo-induced processes are very important from scientific and technological points of view.

Since mid 80s, extensive studies have been conducted on surface photochemistry. An excellent review on the early stage of surface photochemistry has been published by Chuang in 1983.[1] Instead of using ill-characterized adsorption systems, "modern" surface photochemistry employs well-defined adsorption systems, i.e., adsorbates on single-crystal surfaces in ultra-high vacuum. Thus, it is possible to obtain more quantitative information on the photochemistry of adsorbates in specific adsorption states. Exhaustive reviews on surface photochemistry performed by mid 90s have been published by Zhou et al.[2] and Ho.[3]

The main issues in surface photochemistry are the following: how are reactant adsorbates electronically excited and what are photochemical products? The first issue is specific to photochemistry at surfaces, because it is not trivial to know which electronic system, adsorbate or substrate, is excited to initiate adsorbate photochemistry. Regarding the second issue, the angular and energy distributions of desorbed species are of special interest in addition to simple product analysis, because they provide information of potential energy surfaces (PESs) relevant to photo-stimulated desorption (PSD).

Product analysis including detailed measurements of energy distributions of desorbed species is necessary to characterize photochemistry, but these results do not directly provide information on what is really happening at the surfaces in real time. To investigate nuclear dynamics on surfaces initiated by photo-irradiation, we need to develop new spectroscopic tools. Thanks to the advent of recent femtosecond (fs)-laser technology, it has become possible to probe not only nuclear dynamics, but also electron dynamics to some extent.[4–6]

On metal surfaces, in particular, photo-induced processes

Published on the web May 14, 2007; doi:10.1246/bcsj.80.842

provide excellent opportunities to investigate nonadiabatic effects. Since nuclear motions of adsorbates strongly couple to electron motions in metal, strong nonadiabaticity is essential in photochemical processes on metal surfaces. Therefore, it is vital to observe nuclear motions under electronic excitation directly in the time domain for a deeper understanding of nonadiabatic couplings at metal surfaces.

This account describes mainly two major developments in my laboratory in the last decade: photochemistry of saturated hydrocarbons and real-time observations of photo-induced coherent nuclear dynamics of alkali-metal adsorbates on metal surfaces. This account is organized as follows. In Section **2**, we first survey excitation mechanisms in surface photochemistry. In Section **3**, we describe the photochemistry of methane and cyclohexane, mostly focusing on excitation mechanisms. Then, in Section **4**, we describe coherent vibration at alkali-metal adsorption systems using time-resolved second harmonic generation (TRSHG) spectroscopy and some attempt to control the coherent vibration employing tailored fs-pulse trains.

2. Excitation Mechanisms and Nuclear Dynamics in Surface Photochemistry

2.1 Electronic Excitation at Surfaces by Photo-Irradiation. The excitation mechanism in surface photochemistry is not trivial compared to photochemistry in gas and solution phases. In the region of photon energy for excitation of the valence electrons on surfaces, two excitation mechanisms have been frequently quoted in the literature for surface photochemistry:[2,3] adsorbate-localized and substrate-mediated excitations schematically depicted in Fig. 1. In the former mechanism, electronic excitation takes place directly from an occupied electronic state to an unoccupied state that are localized in an adsorbate. This is similar to optical electronic excitation of a molecule in the gas and solution phases. In the latter mechanism, the electronic excitation of an adsorbate is indirect. First, photons are absorbed by a substrate, such as a metal or a semiconductor, to create electron–hole pairs in the substrate. Then, hot electrons or holes created are scattered with adsorbates. If electron (or hole) energy is resonant to an adsorbate unoccupied (occupied) state, the scattering of electrons or holes is resonantly enhanced. In this case, the resonant scattering yields a transient ionic species at the surface, and hence, the electronic configuration of the adsorbate changes.

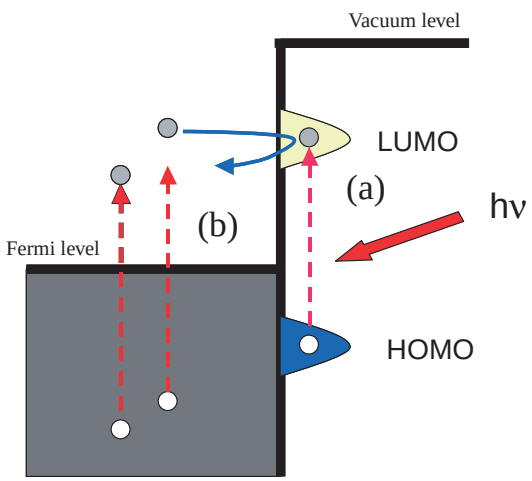

Fig. 1. Excitation mechanisms of photochemistry at metal surfaces. Two excitation schemes are depicted. (a) Adsorbate-localized excitation via direct optical transition from an occupied to an unoccupied state of the adsorbate both localized at the adsorbate. (b) Substrate-mediated excitation via resonant scattering of hot electrons created by photon absorption in the substrate.

Note that the two mechanisms are conceptually different, but distinguishable only in the extreme. In the case of chemisorption, the electronic states of an adsorbate are mixed with those of a substrate. The wave function of the mixed state has a bulk character, so that it is delocalized into the bulk to some extent. Thus, it becomes more difficult to distinguish whether photons excite the adsorbate or the substrate as the degree of mixing increases. However, we can still argue even in the chemisorption case whether or not an electronic transition of interest mainly uses a part of the mixed state wave function at the adsorbate side, if an unoccupied state, such as an image potential state, is involved in the electronic transition, since the mixed-state wave function is projected to the state localized at the surface. In the case of physisorption, the distinction between the two mechanisms may be made more easily. Since the highest occupied molecular orbital (HOMO) of an adsorbate is not significantly altered upon adsorption, this is localized at the adsorbate. If an unoccupied state of the adsorbate, such as the lowest unoccupied molecular orbital (LUMO), is also localized at the adsorbate, the optical transition between the two states is essentially same as an isolated molecule. However, if the unoccupied state is significantly mixed with substrate electronic states, the final state has a delocalized bulk character. In this case, excitation can be viewed as electron transfer from the adsorbate to the substrate, since the transition is made from the adsorbate-localized state to the state whose electronic wave function is delocalized in the bulk. We discuss this type of transition in detail in Section **3**.

2.2 Nuclear Dynamics Induced by Photo-Excitation. Let us discuss how nuclear dynamics in surface photochemistry has been interpreted in the past in terms of models developed for PSD. Desorption induced by electronic transition has been discussed in terms of a simplistic model developed by Menzel, Gomer, and Redhead, i.e., the MGR model[7,8] for electron-stimulated desorption, which is the historical antecedent of PSD. In either excitation mechanism cited in the last section, the PES with respect to an adsorbate–substrate coordinate is altered due to changes in the electronic configuration associated with the electronic excitation of an adsorbate. As depicted in Fig. 2, the adsorbate nuclear wave function in the ground adsorption potential well is projected vertically to the repulsive part of the upper PES. Then, the adsorbate starts to move toward the vacuum and gains some kinetic energy E'_K on the excited-state PES. If the adsorbate gains kinetic energy large enough to surmount an energy barrier for desorption in the ground-state PES D_0 by the time that the adsorbate is quenched electronically, i.e., $E'_K > D_0$, it desorbs from the surface with kinetic energy E_K. If the excited-state lifetime is so short that the adsorbate does not gain enough energy to surmount the desorption barrier, then the adsorbate is recaptured and trapped in the original adsorption potential well. In this case, the adsor-

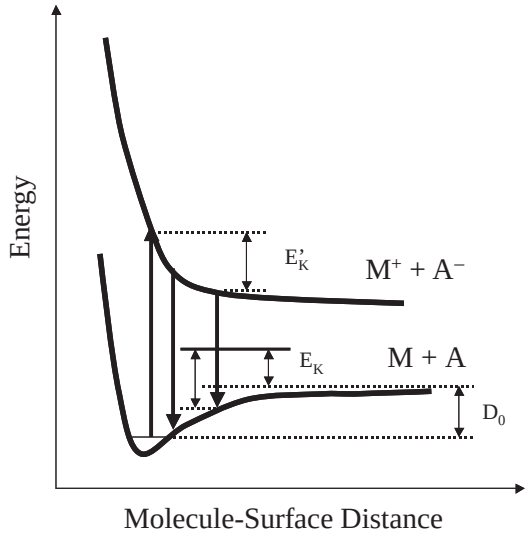

Fig. 2. Schematic potential energy surfaces for the MGR model. First, the adsorbate in the ground state is excited to the repulsive potential energy surface. The excited adsorbate gains some kinetic energy E'_K on the upper potential energy surface and then quenched back to the ground potential energy surface. If the adsorbate stays on the upper potential energy surface long enough to fulfill the condition $E'_K > D_0$, where D_0 is the adsorption energy, it desorbs with the kinetic energy E_K. Otherwise, it is trapped in the ground potential surface again.

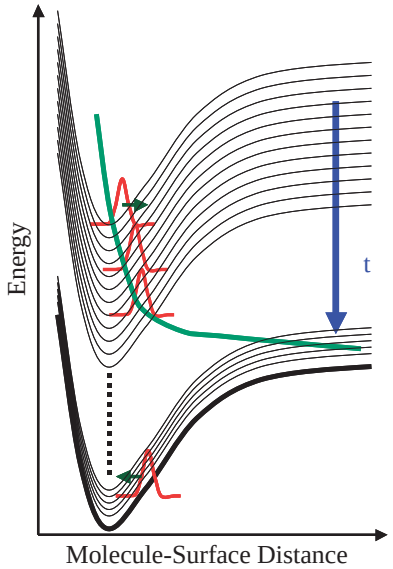

Fig. 3. MGR model in which the electronic relaxation processes are explicitly expressed. The repulsive potential energy surface crosses with a bunch of potential surfaces similar to the ground state adsorption potential owing to electron–hole pair creation in the substrate. Thus, the created wave packet on the repulsive potential surface goes through continuous crossing points. The wave packet crosses to the PES similar to the adsorption potential well starts oscillating in it, if it does not gain enough kinetic energy to overcome the desorption barrier.

bate cannot desorb, but starts vibrating in the adsorption well. Antoniewics[9] has proposed a modified version in which the repulsive upper PES is replaced with a bound PES with its equilibrium position closer to the surface than that of the ground-state PES. This version is frequently used for the ionic excited state formed by substrate-mediated excitation. It is easy to extend these models for bond cleavage of adsorbates, i.e., dissociation, if we use a PES with respect to internal vibration coordinates of the adsorbate.

This model is crude, but easy to grasp major features of PSD. Assuming appropriate time-dependent survival probabilities of adsorbates excited into the upper PES and the shapes of the ground- and excited-PESs, we can account for kinetic energy distributions of desorbed species semi-quantitatively.[10] However, this model might be confusing for chemists working on photochemistry of simple molecules, where cleavage of a bond and subsequent nuclear dynamics occurs on an excited state PES. What does the down arrows, i.e., electronic quenching, in Fig. 2 really mean? The electronic quenching means nonadiabatic transitions that are particularly characteristic of metals. Obviously, there exist an infinite number of PESs other than the two depicted in Fig. 2 for the adsorbate on the metal. On the metal surface, the relaxation of an adsorbate electronic excited state is mainly preceded by electron–hole pair creation in the substrate. Thus, the repulsive PES crosses with a bunch of PESs associated with the electron–hole pair creation as schematically depicted in Fig. 3. Here, the electronic state of the total system including the adsorbate and substrate is taken into account in the adiabatic picture. Consequently, a nuclear wave packet, created on the repulsive PES by photo-excitation, crosses to a bound PES during the electronic relaxation. This crossing from one PES to the other implies electronic quenching expressed as the down arrow in Fig. 2. Since most of energy dissipation processes due to electron–hole pair creation in the bulk are not relevant to the interaction between the adsorbate and substrate, the topological features of PESs crossing the repulsive PES are very similar to those of the ground state. This is why desorption dynamics are described with two PESs in the generic MGR model. Therefore, although the generic MGR model uses only one PES, which is the lower PES depicted in Fig. 2, to describe nuclear dynamics for both initial and final states in the PSD process, the lower PES actually represents the ground-state PES in two situations: before electronic excitation takes place and while the adsorption system is still electronically exited.

The strong nonadiabatic couplings between electrons and nuclear motions are the essence of metal that determine many physical properties of metals. Photo-induced nuclear dynamics are no exception. The significance of nonadiabatic couplings has been extensively discussed recently in various processes induced by ultrashort laser pulses, including desorption induced by multiple electronic transitions (DIMET),[11] femtochemistry on metal surfaces,[5,12,13] frustrated photodesorption of alkali-atoms from noble metals,[4,14] and dynamics of coherent surface phonons[6,15–17] that we describe in detail in Section **4**.

3. Photochemistry of Saturated Hydrocarbons

Although saturated hydrocarbons, such as methane, in the gas phase absorb vacuum ultraviolet photons, they are transparent to visible and ultraviolet (UV).[18] Thus, no UV–visible

photochemistry takes place in the gas phase. In contrast, we demonstrated that methane weakly adsorbed on metal surfaces is readily dissociated with irradiation of 6.4-eV photons.[19–24] Methane is a typical physisorption system on metal surfaces, such as Pt and noble metals, and CH-bond cleavage is a thermally activated process on these surfaces. Thus, it is clear that the dissociation upon UV irradiation is nonthermal and is induced by electronic excitation. A problem is that methane is dissociated with photons with energies that are much less than the first allowed transition of methane in the gas phase. Moreover, there is another problem involving saturated hydrocarbon adsorption on metal surfaces, i.e., "CH vibrational mode softening."[25–34] Saturated hydrocarbons adsorbed on metal surfaces show that one of CH stretching absorption bands is significantly redshifted. In this section, the electronic excitation mechanism of the photochemistry of small saturated hydrocarbons, i.e., methane and cyclohexane, is discussed together with a plausible origin for the CH vibrational mode softening.

3.1 Electronic Structure of Saturated Hydrocarbons. Electronic excited states of neutral methane are relevant to the photochemistry of methane in the case of adsorbate-localized excitation, whereas transient negative ion states are relevant to the case of substrate-mediated excitation. First, we describe the electronic structure of methane as a representative example of saturated hydrocarbons. The electronic structure of saturated hydrocarbons is characterized by high lying excited states because there are no π electrons. Thus, CH σ^* states are "buried" in series of Rydberg states.[35] The electronic configuration for the ground state of methane is $(1a_1)^2(2a_1)^2(1t_2)^6,{}^1A_1$. The first excited state of methane in the gas phase, $(1t_2 \rightarrow 3sa_1^1)$ $({}^1T_2)$, is located at $\approx$10 eV above the ground state. The excited-state orbital is essentially a 3s Rydberg-type orbital. Excitation to the excited states leads to dissociation of methane to $CH_2 + H_2$ and $CH_3 + H$, which has been studied experimentally[18,36–39] and theoretically.[40–42] Recent ab initio calculations[42] and experiments[38,39] suggest that photodissociation of gaseous methane occurs after intersystem crossing to the T_1 state or internal conversion to the S_0 ground state.

Transient negative ion states of methane have been investigated with various methods, including direct electron transmission spectroscopy, electron scattering, and dissociative attachment studies.[35] The resonance feature at an electron energy of $\approx$10 eV has been unambiguously assigned to the lowest Feshbach resonance, $(1t_2 \rightarrow 3sa_1^2),{}^2T_2$. The transient negative ion state proceeds to dissociation to CH_3 and H^-. Below this electron energy, the assignments of resonance features are not necessarily clear. However, these resonance features are all related to inelastic scattering, such as vibrational excitation, but no dissociative electron attachment has been observed.

3.2 Adsorption State of Saturated Hydrocarbons on Metals. As stated earlier, the adsorption of small saturated hydrocarbons on late transition and noble metal surfaces are weak, i.e., physisorption. However, there are some indications showing saturated hydrocarbons interact with the metal surfaces more specifically.

For methane adsorption on Pt(111), Yoshinobu et al.[43] have observed that methane in the first layer has an infrared (IR) absorption band that cannot be assigned to methane with T_d symmetry. Gaseous methane has two CH stretching modes: degenerate stretching (ν_3) at 3019 cm^{-1} and symmetric stretching (ν_1) at 2917 cm^{-1}. If adsorbed methane has T_d symmetry, only the ν_3 band should appear in IR spectra according to the surface dipole selection rule. In contrast, two absorption bands at 2997 and 2882 cm^{-1} have been observed in the CH stretching range of the IR spectra of methane adsorbed on Pt(111). While the absorption band at 2997 cm^{-1} has been assigned to ν_3, the band at 2882 cm^{-1} has been assigned to the ν_1 mode that can only be observed if methane has symmetry lower than T_d, such as C_{3v}, C_{2v}, etc. This clearly indicates that the symmetry of methane is lowered due to adsorbate–substrate interaction.

Another indication of the interaction between saturated hydrocarbons and metal substrates is CH vibrational mode softening. A CH stretching band has been shown to significantly broaden and redshift from the other symmetric and anti-symmetric CH stretching bands for cyclohexane on Ni(111) and Pt(111).[25] The origin of the CH vibrational mode softening has been extensively discussed in the past. Raval et al.[26–28] have suggested that a hydrogen-bonding-like interaction exists between a metal surface and CH groups, which lie in close proximity to it. This interaction is understood in terms of two-way electron transfer from a bonding CH σ orbital to unoccupied metal orbitals and from occupied metal orbitals to an antibonding CH σ^* orbital. As we discuss in detail in Section **3.4**, Wöll and co-workers have proposed the existence of hybrid orbitals between the hydrocarbon and the metal substrate on the basis of C1s near edge X-ray absorption fine structure (NEXAFS) studies of saturated hydrocarbons on metal surfaces.[29–31] With the aid of ab initio calculations on cyclopropane[32,33] and cyclohexane on Cu(111),[33,34] they showed that the hybridization is due to the back-donation of electrons into the adsorbed alkane instead of the two-way electron transfer.

3.3 Photochemistry of Saturated Hydrocarbons. Photochemistry of methane adsorbates was studied with post-irradiation temperature-programmed desorption (TPD) and X-ray photoelectron spectroscopy (XPS). Figure 4 shows TPD results. A Pt(111) surface was first saturated with methane to form a monolayer and then irradiated with 6.4-eV photons at the surface temperature of 40 K. A TPD result before laser irradiation is depicted in Fig. 4a; only the molecular desorption peak denoted as α was observed. In contrast to the pre-irradiation TPD result, the post-irradiation TPD result in Fig. 4b showed a depleted α-desorption peak, while a new peak denoted as β at around 260 K. The β peak was attributed to the associative recombination of CH_3 and H.[44–46] Moreover, methyl and methane desorbed species were detected by use of a mass spectrometer and their kinetic energy distributions were measured. Thus, it was clear that methane dissociated into methyl and hydrogen as a result of the irradiation of 6.4-eV photons.

Key information for the excitation mechanism can be obtained from the polarization and incident angle dependence of photochemical cross sections.[21,23] If excitation is due to the optical transition localized at the adsorbate, the cross section should be proportional to $|\vec{\mu}\cdot\vec{E}|^2$, where $\vec{\mu}$ is a transition dipole moment fixed to the molecular frame and $\vec{E}$ is the electric vector of the excitation light at the surface. In contrast, if the excitation is due to hot electron transfer from the surface to the adsorbate following the creation of electron–hole pairs due

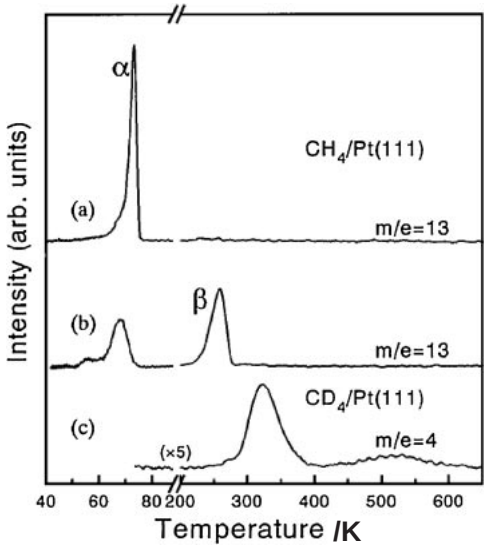

Fig. 4. Temperature-programmed desorption (TPD) results of methane: (a) before and (b) after irradiating 6.4-eV photons onto Pt(111) saturated with CH_4. The α peak is due to molecular desorption of methane, whereas the β peak is due to associative recombination of CH_3 and H. (c) Post-irradiation TPD result of D_2 from Pt(111) saturated with CD_4. A weak broad peak at around 550 K is due to further thermal decomposition of CD_3 created by photodissociation of CD_4. The appearance of the β and D_2 peaks clearly indicates that methane is photolyzed to methyl and hydrogen upon 6.4-eV photon irradiation. Reprinted with permission from Ref. 21. Copyright 1996, The American Institute of Physics.

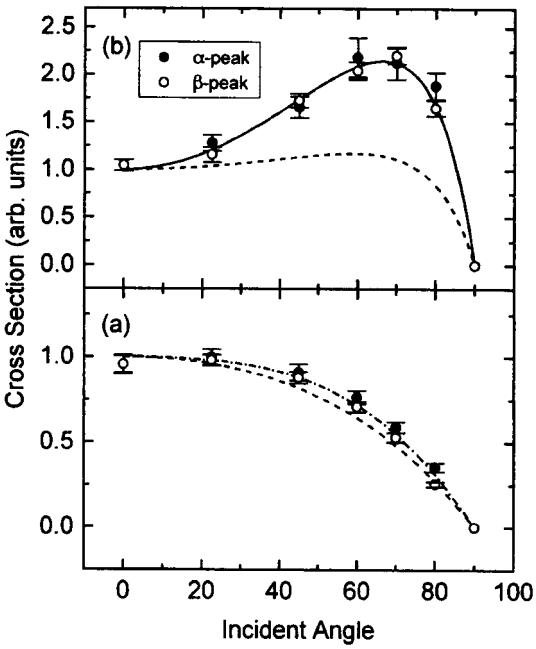

Fig. 5. Polarization and incident-angle dependence of cross section for methane photochemistry. The cross sections are estimated from the peak intensity of the α (solid circle) and the β (open circle) desorption peaks as a function of the number of photons irradiated. The impinging light at 6.4 eV is polarized (a) perpendicular (s polarization) and (b) parallel (p polarization) to the plane of incidence. The dashed curves are calculated absorbance of the platinum substrate. The dash-dotted curve in the lower panel is the square of electric field strength of the component parallel to the surface. The solid curve in the upper panel is calculated result under the assumption that the transition dipole tilting from the surface normal by 66°. Reprinted with permission from Ref. 23. Copyright 1996, The American Physical Society.

to absorption of photons by the substrate, the cross section is proportional to the absorbance of the substrate. Effective photochemical cross sections are plotted in Fig. 5 as a function of incident angle of linearly polarized light. The cross sections were estimated from the peak intensity of the α (solid circle) and the β (open circle) desorption peaks in Fig. 4 as a function of the number of photons irradiated. The dashed curves are calculated absorbance of the platinum substrate. The dash-dotted curve in the lower panel is the square of electric field strength of the component parallel to the surface. The solid curve in the upper panel is the calculated result under the assumption that the transition dipole tilts from the surface normal by 66°. The results of p-polarized light clearly deviated from the absorbance of the substrate, implying that the excitation cannot be explained in terms of the substrate-mediated mechanism; a transition dipole moment perpendicular to the surface is involved in the excitation. This experimental result strongly suggested that adsorbate-localized states are involved in the excitation.

Photochemistry of cyclohexane on Cu(111) was similar to that of methane on metal surfaces.[47] Cyclohexane weakly adsorbed on Cu(111) and molecularly desorbed at 180 K. No thermal dissociation took place on this surface. Upon 6.4-eV photon irradiation, TPD and XPS results indicated that cyclohexane dissociated into a cyclohexyl moiety and hydrogen. The cyclohexyl moiety was further dehydrogenated by annealing the surface to produce cyclohexene that desorbed at 230 K. The incident-angle dependence of photochemical cross sections of cyclohexane in the case of p-polarized light irradiation also deviated greatly from that of substrate absorbance. Therefore, neither of methane and cyclohexane photochemistry on the metal surfaces can be understood in terms of the substrate-mediated excitation mechanism; rather electronic states localized at the adsorbates play an important role in the electronic transitions.

3.4 Interactions between Saturated Hydrocarbons and Metal Surfaces. Theoretical calculations on electronic excited states of adsorbates, including saturated hydrocarbons, such as methane and cyclohexane, on metal surfaces are scarce. Hirao and co-workers have conducted ab initio calculations of electronic states of methane–Pt_n ($n = 1$ to 10) clusters.[48] The adsorption geometry in the ground state can be calculated by means of density functional theory (DFT). Then, excited states are calculated using the state-averaged complete active space self-consistent field (SA-CASSCF) method. These calculations properly predict a transition energy of 10 eV from the ground to the first excited state of gaseous methane. Moreover, the SA-CASSCF calculations indicate that the first excited state of methane with a Rydberg character interacts with unoccupied states of Pt_n strongly. As a result, the first excited

state of methane results in a charge-transfer state and stabilized by ≈3 eV compared with gaseous methane. Similar behavior has been found on Ni and Pd clusters.[49] Thus, the calculations demonstrate the excited state of methane mixes with metal states more strongly than the ground state.

Other clues for the interactions between saturated hydrocarbons and metal surfaces come from experiments. Wöll and co-workers[31,32] have measured C1s NEXAFS of various saturated hydrocarbons. The NEXAFS spectrum of multilayer cyclohexane on Cu(111) shows three resonances characteristic of saturated hydrocarbons: Rydberg resonance at 288.0 eV, $CC_{\sigma*}$ resonance at around 293.1 eV, and CC′ resonance at 301.0 eV. These features, in particular, the Rydberg resonance peak, are significantly altered for monolayer cyclohexane as well as other saturated hydrocarbons. Namely, three new features appear: a broad feature at 258.1 eV (M* resonance) and two sharp features located at 286.9 (R′ resonance) and 288.9 eV (R″ resonance). The M* resonance is located at just above the threshold for excitations into empty states of metal. Thus, the M* state is assigned to transitions into unoccupied electronic states that are formed upon the adsorption of cyclohexane through a hybridization between molecular and substrate electronic states, whereas the sharp R′ and R″ resonances have been assigned to molecular Rydberg states.

Nilsson and co-workers have also found a mixed band right above the Fermi level E_F using X-ray absorption spectroscopy (XAS) for *n*-octane on Cu(110).[50,51] This M* band is apparent when the p electronic structure is probed along the surface normal. In addition, X-ray emission spectroscopy indicates that an additional feature due to an occupied p_z state at 5 eV below E_F. This feature is denoted as M. With the aid of DFT calculations, they have shown that the M and M* states are induced by the hybridization between molecular orbitals of *n*-octane and the metal d band. Namely, the interaction with the d band contributes to the bonding, which brings the molecule closer to the surface, and increases the rehybridization of the molecular orbitals, resulting in CH bond elongation.

The same group has recently reported XAS results and DFT calculations on methane on a Pt(977) surface.[52] Although this surface is composed of steps and (111) terraces, it has been confirmed that approximately 10% of the surface atoms at the steps do not significantly affect the adsorption state of methane. Figure 6 shows XAS spectra around the C K-edge. Note that the XAS spectrum taken with X-ray light, of which the electric vector is out of the surface plane (solid topmost spectrum), clearly shows the transition to the gas-phase LUMO level and more importantly the transition to the M* state extending to the Fermi level. The appearance of the transition to the LUMO level indicates that the symmetry of methane is broken at the surface, otherwise this transition is symmetry forbidden. As stated earlier, this adsorption-induced symmetry lowering has also been detected in the IRAS measurements.[43] The appearance of the transition to the M* state has been interpreted as the rehybridization between the bonding and antibonding orbitals of methane due to the interaction with the metal. The DFT calculations on the configuration where one of CH bonds points to the surface indicate that an increase of electron density at the C and a decrease at the H atom in the adsorbed methane. However, there is only little increase

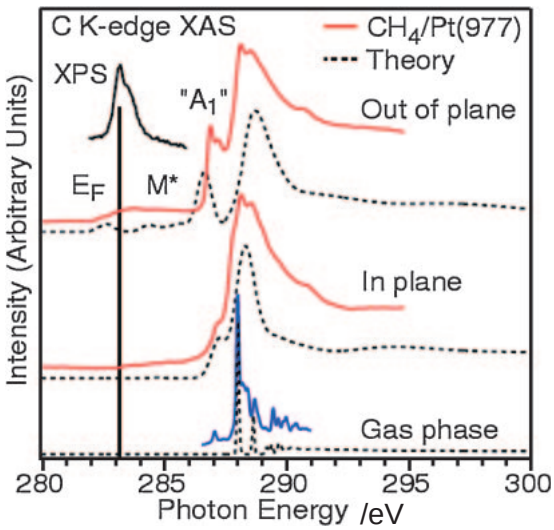

Fig. 6. X-ray absorption spectra of methane adsorbed on a Pt(977) surface. The spectra with solid lines show from the top: taken with the *E* vector out or the surface plane, *E* vector in the surface plane, and gas-phase methane from Ref. 82. The dashed lines show the corresponding computed spectra, shifted 2.3 eV towards lower energy to match the experimental energy scale. An XPS spectrum is shown to give the position of the Fermi level depicted a long vertical line. Reprinted with permission from Ref. 52. Copyright 2006. The American Physical Society.

of electron density between the molecule and the metal. Thus, there is no adsorbate–substrate covalent bonding, but the electron density is polarized as a result of mixing with CH-antibonding p character to minimize Pauli repulsion upon adsorption. The elongation of the CH bond by 0.09 Å has been estimated in comparison the XAS spectrum with the theoretically simulated spectrum.

These findings suggest the following excitation mechanism in the photochemistry of methane and cyclohexane on the metal surfaces that takes place at the photon energy much lower than the onset of absorption in the gas phase. The chemical interactions between the saturated hydrocarbons and metal surfaces and the rehybridization among the electronic states of methane manifest themselves in the hybridized bands across E_F, M and M*. Thermal occupation of these bands causes the symmetry reduction of methane and substantial softening of the CH stretching mode of cyclohexane. Moreover, the unoccupied M* band at E_F makes transitions from HOMO levels of adsorbates possible. Since the onset of HOMO is located at ≈5 eV, the M* state can be excited from the HOMO with 6.4-eV photons.

Since the hybridized M* state has a metallic character largely on one hand and the HOMO state is localized at the adsorbate on the other, the transition relevant to the photochemistry is probably photo-induced electron transfer from the hydrocarbon adsorbates to metal substrates. Figure 7 shows the energetics of photochemistry of methane on Pt(111). The adsorption energy of methane is ≈0.5 eV. The ionization potential of gaseous methane is 12.6 eV. When a methane cation is located at the equilibrium distance of a neutral methane from the Pt sur-

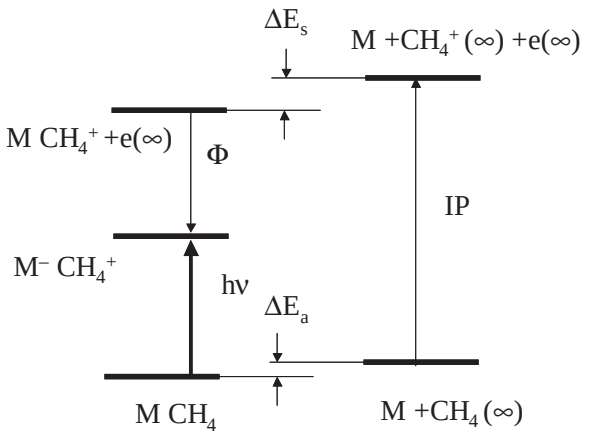

Fig. 7. Energetics of methane photochemistry. Here, M and M^- denote platinum in the neutral condition and with an excess electron from methane, respectively. IP is the ionization potential of methane, Φ is the work function, ΔE_a is the adsorption energy of methane, and ΔE_s is the stabilization energy due to Coulombic attraction between CH_4^+ and its counter charge in the metal. $CH_4(\infty)$ and MCH_4 denote that methane is located in the vacuum far from the surface and at the adsorption equilibrium position, respectively.

face, the energy of the cation is lowered by Coulombic attraction between the cation and its counter charge in the metal. This energy has been estimated to be 1.9 eV at a distance of 0.3 nm from the metal surface. Then, bringing an electron from infinite distance into the metal substrate leads to stabilization of the cation by the work function of the system, (5.6 eV). Therefore, the net energy necessary to produce the electron-transfer state of the cation is less than 5.6 eV. If the stabilization energy of the excited state due to the specific hybridization is taken into account, the threshold energy should become smaller. This simple-minded picture provides the energetics of the photochemistry associated with the photo-induced electron transfer from methane to Pt substrate semi-quantitatively.

4. Coherent Surface Phonons on Metal Surfaces

Considerable efforts have been made to understand angular and energy distributions of desorbed species upon photo-irradiation in the past,[10] which provides some clues to the nuclear dynamics of adsorbate at surfaces and the topology of the PES relevant to desorption. In contrast to the extensive studies on desorbed species, photo-induced real-time nuclear dynamics have been mostly unexplored. As described in Section **2**, the electronic excited states of adsorbates on metal surfaces suffer from rapid electronic relaxation. Thus, nuclear dynamics toward desorption (or dissociation) of adsorbates compete with the rapid electronic relaxation. Generally, since the electronic relaxation takes place more rapidly than nuclear motions of adsorbates, the majority of nuclei can not gain kinetic energy large enough to surmount the barrier for desorption. Thus, the quantum yields of photochemistry on metal surfaces are usually very small. Although the majority of adsorbates that are excited cannot escape from the adsorption well, they gain some kinetic energy and start to vibrate. In order to understand the nuclear dynamics induced by photon excitation, it is important to study the major channel of photo-induced processes. For this purpose, it is necessary to develop ultrafast spectroscopy to monitor photo-induced vibrational dynamics on metal surfaces directly.

We developed time-domain nonlinear spectroscopy, i.e., time-resolved second harmonic generation (TRSHG) spectroscopy, for studying the photo-induced nuclear dynamics at surfaces. If adsorbates undergo nonthermal nuclear motion randomly as a result of photo-excitation, it is very hard to extract dynamical information from an ensemble of adsorbates. However, if the duration of a pump pulse is sufficiently shorter than the time scale of nuclear motion of interest, for example, adsorbate–substrate vibration, the pump pulse creates a nuclear wave packet for each adsorbate in phase in the electronic excited state; the nuclear motion is excited coherently. In this case, we can learn nuclear dynamics in the time domain by probing the macroscopic polarization created in the ensemble of adsorbates. For studying nuclear dynamics at surfaces, SHG is a natural choice of methods, since SHG is sensitive to surfaces and interfaces.[53]

In this section, we focus on the excitation and evolution of coherent surface vibrational motions of alkali-metal atoms on metal surfaces. In Section **4.1**, we describe excitation and detection methods of coherent motions. After summarizing the electronic structure of alkali-metal atoms on metal surfaces in Section **4.2**, we describe experimental results of Cs on Pt(111) in Section **4.3** and selective excitation of a phonon mode by using tailored pulse trains in Section **4.4**.

4.1 Excitation and Detection of Vibrational Coherence at Metal Surfaces. Interactions between quantum systems with ultrafast laser pulses can be described by using the time evolution of the density operator. The density operator evolves in terms of the radiation–matter interaction, $H_{\mathrm{int}} = -\int \vec{E}(\vec{r},t)\cdot\vec{P}(\vec{r},t)\mathrm{d}\vec{r}$, where $\vec{E}(\vec{r},t)$ is the electric field of light and $\vec{P}(\vec{r},t)$ is the polarization density of the matter. In a perturbation approach, the time-dependent density operator $\rho(t)$ is expanded in powers of the electric field,[53,54]

$$\rho(t) = \rho^{(0)}(t) + \rho^{(1)}(t) + \rho^{(2)}(t) + \ldots, \quad (1)$$

where $\rho^{(0)}$ is the density operator for the system at thermal equilibrium and $\rho^{(n)}$ is the n-th order contribution in an electric field. Here, we only focus on the second-order contribution $\rho^{(2)}(t)$, because it is the most relevant to the spectroscopy described in this account.

Figure 8 shows possible schemes for creation of vibrational coherence originating from the second-order contributions. These schemes are all called impulsive stimulated Raman scattering (ISRS).[55] Note that off-diagonal terms of the density matrix are responsible for excitation of coherent oscillations, rather than diagonal terms. These off-diagonal terms formed by a pump pulse are the origin of a macroscopic polarization oscillating with the frequency of a coherent phonon mode. The created coherence and its dephasing are detected through the interaction between the polarization of the medium and the electromagnetic field of a probe pulse. An important requirement for creation of vibrational coherence is that a pump-pulse duration should be much shorter than the vibrational period of interest. In other words, the coherent spectral width of the pump pulse should exceed the vibrational frequency.

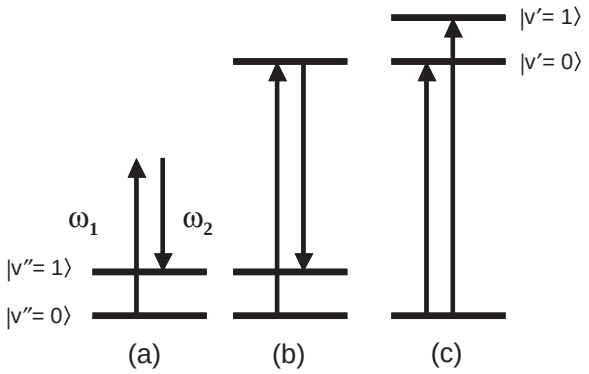

Fig. 8. Creation of vibrational coherence in terms of impulsive stimulated Raman scattering. (a) Off-resonant and (b) and (c) resonant cases with respect to an electronic transition. See the text for distinction between (b) and (c) for adsorbates on metal surfaces. The pumping laser pulse should have a broad coherent spectral width covering the frequency components of $\omega_0 = \omega_1 - \omega_2$, where ω_0 is the vibrational frequency of interest.

Scheme (a) represents ISRS without electronic resonance. If the excitation pulse has a broad spectral width, stimulated Raman scattering occurs as a result of mixing the frequency components ω_1 and ω_2, fulfilling the vibrational resonant condition $\omega_1 - \omega_2 = \omega_0$, where ω_0 is the vibrational frequency. That is, the duration of the pump pulse has to be less than the vibrational period for impulsive Raman excitation. This excitation process is substantially enhanced when the excitation energy is near an electronic absorption resonance, which is depicted in scheme (b). In this electronic resonance case, coherent vibrational motion can be initiated also in the electronically excited state if the pump-pulse duration is substantially shorter than the excited-state vibrational period, as depicted in scheme (c).

The distinction between the evolution of vibrational coherence in the ground (scheme (b)) and excited (scheme (c)) states is very clear in molecules, since the electronic excitation of a molecule, in which electrons are localized in a limited space, results in a profound change in PESs. In contrast, the deformation potentials for ions in solids and on surfaces hardly change upon excitation in the weak excitation region where the perturbation treatment is valid. Thus, the distinction between schemes (c) and (d) of resonant ISRS may not be practically meaningful in this region. The distinction would be more clear if the density of excited carriers became so high that the deformation potentials were significantly altered. However, in the strong excitation region, the perturbation treatment is no longer valid.

In addition to the resonant ISRS excitation mechanism, a phenomenological excitation scheme, called displacive excitation of coherent phonons (DECP), has been frequently discussed.[56–58] In this mechanism, real populations of electrons (holes) in an empty (occupied) band are assumed to change the deformation potential of ions in solids and at surfaces. If a pump pulse produces electrons (holes) in an empty (occupied) band with a sufficiently rapid rising edge, the ions cannot follow the change in the deformation potential and start to oscillate around new equilibrium positions. Note that the oscillator energy is modified through a change in potential energy in the DECP mechanism. In contrast, the kinetic energy is transferred to the oscillator by the real driving force in the case of nonresonant impulsive Raman excitation.[59] The DECP model predicts a cosine-like initial phase of coherent oscillation, but only accounts for the generation of totally symmetric phonon modes in the electronic excited state.[56,57]

Since the DECP mechanism is intuitive and simple, this mechanism has been applied to generation of coherent phonons in various semiconductors and semimetals.[58] However, note that the electromagnetic field of a pump pulse provides only the energy for electronic excitation from the ground to excited states in the DECP mechanism. This mechanism does not explicitly implement creation of nonzero off-diagonal terms in the density matrix of the system as a source of coherence. In this context, the DECP mechanism is phenomenological. In spite of the lack of rigorous treatment for coherence, the DECP mechanism is practically useful for cases of strong electronic excitation, to which the second-order perturbation treatment is no longer applicable.

When a surface phonon mode is coherently excited by a pump pulse, non-stationary coherent nuclear motions modulate electronic degrees of freedom. Thus, the second-order optical susceptibility $\chi^{(2)}(2\omega)$ and, hence, macroscopic polarization $P^{(2)}(2\omega)$ are modulated by the coherent motions. Since this modulation is small, $\chi^{(2)}$ can be expanded at the equilibrium position of a nuclear coordinate $Q = Q_0$ relevant to the coherent oscillation in terms of nuclei displacement δQ as

$$\chi^{(2)} = \chi^{(2)}|_{Q=Q_0} + \left.\frac{\partial \chi^{(2)}}{\partial Q}\right|_{Q=Q_0} \cdot \delta Q + \ldots . \qquad (2)$$

Because SH intensity is proportional to $|\chi^{(2)}|^2$, the leading term of the modulation due to the coherent oscillation is a cross term between the first and second terms in Eq. 2. Thus, the time-evolution of the coherent oscillation can be detected by measuring the difference in SHG intensity of a probe pulse between with and without a pump pulse as a function of t.[17]

The procedures for TRSHG measurements are described in detail elsewhere.[15–17] Either a Ti:sapphire regenerative amplifier (Spectra Physics, Spitfire, 1 kHz) or a home-built non-collinear optical parametric amplifier (NOPA) pumped by the regenerative amplifier was used for TRSHG measurements. The pulse duration of pump and probe pulses from the regenerative amplifier was 150 fs and from the NOPA 25 fs. The SH intensity of a probe pulse was detected by using a photomultiplier tube as a function of pump-probe delay t. An optical chopper was inserted in the optical path of the pump pulse for detection of pump-induced SH intensity modulations. In order to extract SHG signals modulated by a pump pulse, we measured transient changes of SH intensity ΔSH defined as $\Delta SH(t) = (SH(t) - SH^0)/SH^0$, where $SH(t)$ and SH^0 are SH intensities with and without pump pulses, respectively.

4.2 Electronic Structure of Alkali-Metal Atoms on Metal Surfaces. The geometric and electronic structures of alkali atoms on metal surfaces have been extensively studied and many reviews[60–64] have been written on this subject. Alkali-metal adsorbates show a variety of adsorption structures on metal surfaces, and the superstructures depend on the combination of alkali atom and metal substrate, alkali atom cover-

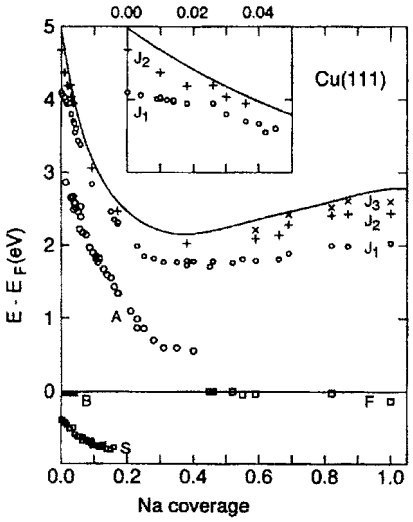

Fig. 9. Electronic structure of a Na-covered Cu(111) surface as a function of Na coverage observed with 2PPE. The coverage denoted here is normalized at the saturation coverage of 4/9 ML. The vacuum level is indicated by the solid line. The inset shows the region of small coverage. Reprinted with permission from Ref. 68. Copyright 1994, Elsevier Ltd.

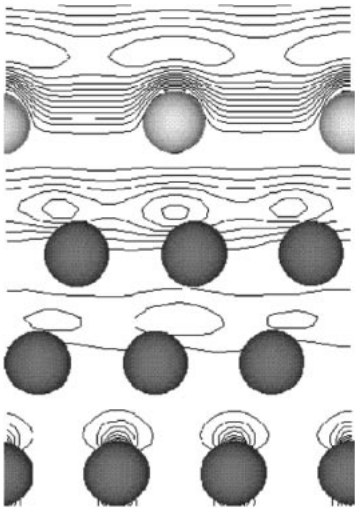

Fig. 10. Local density of states of the quantum-well state at the $\bar{\Gamma}$ point for the saturated monolayer of Na on Cu(111) obtained by using the first-principles DFT calculations. The Cu atoms are dark gray and the Na atoms are light gray. Note that the peak amplitude is localized at the boundary between the Na layer and the vacuum boundary and the amplitude decays rapidly into the Cu substrate. Reprinted with permission from Ref. 70. Copyright 2000, The American Physical Society.

age, and surface temperature. These structures have been reviewed comprehensively by Diehl and McGrath.[64] For example, a phase diagram of K on Pt(111) has been obtained from LEED pattern observations.[65] Below $T \approx 200$ K, the $(\sqrt{7} \times \sqrt{7})R19.1^\circ$ structure appears in the narrow coverage range around $\theta = 0.14$ ML. In the coverage range $0.2 < \theta < 0.4$ ML, the LEED pattern changes to diffraction rings, indicating a reasonably well-defined nearest-neighbor distance, but no long-range rotational correlations in these dispersed overlayers. As the coverage increases, hexagonal super-structures appear, including (2×2) and $(\sqrt{3} \times \sqrt{3})R30^\circ$. As discussed later, the formation of the super-structures allows the observation of coherent surface phonon modes of the metal substrate in addition to the stretching mode of alkali atoms with respect to the metal surface.

Knowledge of the electronic structure of alkali-atom-covered metal surfaces is vital for clarifying the excitation mechanism for coherent motions under fs-laser pulse irradiation. It is well known that the work function of metal is greatly affected by alkali-atom adsorption. The work function of a bare metal surface decreases significantly at low coverages. As the coverage increases, the work function increases slightly and levels off eventually at higher coverages. The traditional explanation of this behavior has been provided by Gurney.[66] In this picture, partial s-electron donation takes place from alkali atoms to the metal surface at low coverages, thereby the bonding of the alkali atom with the metal becomes ionic. This makes a large dipole layer responsible for the significant decrease in the work function. As the coverage increases, repulsive dipole–dipole interactions become prominent and mutual depolarization of the dipoles decreases the net charge of the charge transfer per adatom. At high coverages, the orbital overlap of the alkali atoms is large enough that the alkali overlayer becomes metallic.

Fischer et al.[67,68] have studied the electronic structure of Na on Cu(111) as a function of Na coverage using two-photon photoemission (2PPE), as shown in Fig. 9. At the saturation coverage, the Na overlayer has a hexagonal $(3/2 \times 3/2)$ structure, corresponding to a coverage of $\theta = 4/9 \approx 0.44$ ML.[69] Note that the coverages shown in Fig. 9 are normalized at the saturation coverage. A series of unoccupied states near the vacuum level follow the work function changes.[68] Furthermore, an adsorbate-induced state has also been identified in the 2PPE measurements. While the adsorbate-induced state is unoccupied at low coverages, this state is stabilized and located below E_F at high coverages. Thus, the 2PPE studies clearly show that the bonding nature changes with coverage.

Hellsing and Carlsson have performed first-principles calculations on high coverages of Na on Cu(111).[70] As shown in Fig. 10, the local density of states of the occupied state at $\bar{\Gamma}$ has a maximum in the interfacial region between the Na overlayer and the vacuum barrier and a smaller maximum at the interface between the overlayer and the substrate. As expected, this amplitude decays rapidly into the substrate. They have found that Na-induced bands are located at 0.45 and 2.36 eV above E_F for (2×2) and 0.06 eV below E_F for $(3/2 \times 3/2)$. In fact, the two Na-induced bands for (2×2) have been confirmed later in the STS measurements.[71] Therefore, it is concluded that the Na overlayer forms a metallic quantum well between the barriers of the metal surface and the vacuum, which is also expected to be formed for other combinations of alkali-atoms and metal substrates.

4.3 Coherent Surface Phonons at Alkali-Covered Pt(111) Surfaces. The lower panel of Fig. 11 shows the intensity variation of SH° of 800-nm pulses while Cs was continuously deposited onto a clean Pt(111) surface. The changes in work

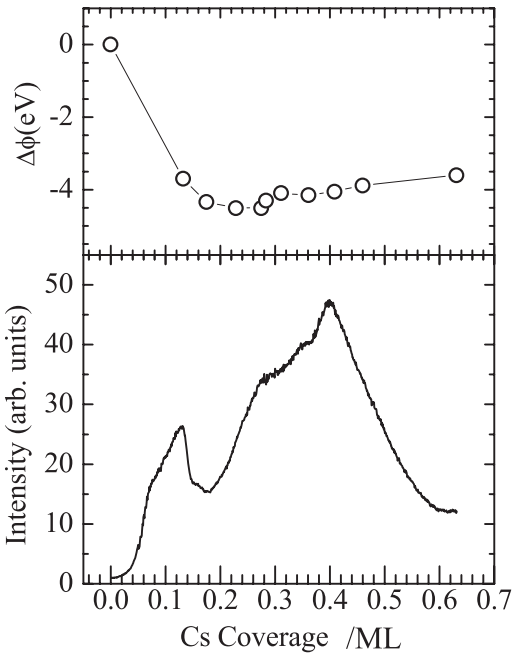

Fig. 11. Variations in SH intensity (solid curve) and work function changes $\Delta\phi$ (circles) as a function of Cs coverage. The wavelength of the excitation laser is 800 nm. Reprinted with permission from Ref. 17. Copyright 2005, The American Physical Society.

function are also plotted in the upper panel. The work function decreased steeply in the beginning of Cs deposition and reached a minimum at a coverage of $\theta \approx 0.25$ ML (1 ML = 1.5×10^{15} cm^{-2}). The SH intensity was remarkably enhanced with the Cs deposition and had strong maxima at ≈0.12 and ≈0.4 ML.

The prominent peak at $\theta \approx 0.12$ ML in Fig. 11 could be due to a two-photon resonance transition between Cs-induced occupied and unoccupied states as in the case of Cs on Cu(111) observed by Lindgren and Walldén.[72] The weak hump at $\theta \approx 0.28$ ML was likely due to a one-photon resonance transition between the Cs-induced states, since the vacuum level was lowered to ≈1.5 eV above E_F at this coverage. At $\theta > 0.28$ ML, the SH intensity increased with θ owing to the local-field enhancement at the adsorbate-vacuum interface and/or the interband transitions between the Cs-induced states.[72,73] As described earlier, the Cs overlayer became metallic in this coverage region similar to Na/Cu(111). Thus, the Cs-induced states involved in the SH enhancement were likely the ones in a quantum well confined within the Cs layer. At $\theta > 0.4$ ML, the SH intensity decreased rapidly, indicating that the photon energy deviates from the exact resonance of the interband transition.

When a Pt(111) surface covered with 0.25-ML Cs was irradiated with 150-fs laser pulses at 800 nm, we found by using TRSHG measurements that coherent vibration of the Cs–Pt stretching mode is generated.[15] Figure 12 shows TRSHG traces taken from clean and Cs-covered Pt(111) surfaces. The TRSHG trace from the clean surface had an instantaneous sharp rise immediately after the excitation. This was followed by a rapid decaying component ($t_d < 1$ ps) and a slowly decaying one ($t_d > 1$ ps). The TRSHG trace showed a similar temporal response of the transient temperature of electrons in the bulk. Thus, hot electrons generated by a pump pulse give major contributions to the TRSHG signals at a clean surface.

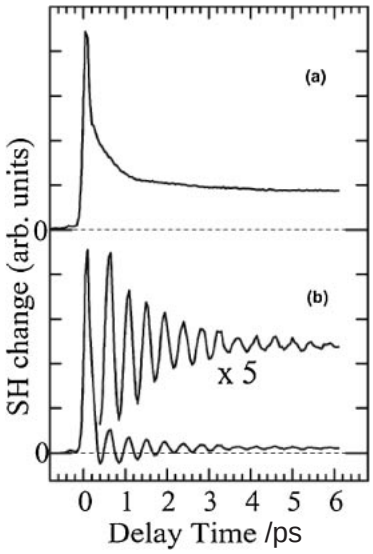

Fig. 12. TRSHG traces for (a) clean and (b) 0.25-ML Cs covered Pt(111) surfaces. A clear oscillatory component of 2.3 THz is seen in (b). The vertical scales are normalized at each peak of the TRSHG trace. Reprinted with permission from Ref. 15. Copyright 2002, Elsevier Ltd.

When Cs coverage was increased, the second harmonic intensity strongly increased due to adsorption of Cs compared with the clean surface. More importantly, clear oscillatory signals appeared in TRSHG traces after the strong peak at $t = 0$. The oscillatory part could be fit to a single underdamped oscillator with a frequency of 2.30 THz (76.7 cm^{-1}) and a damping constant of 1.39 ps. The frequency of the oscillatory signal was close to those of the Cs–substrate stretching vibrational mode of Cs/Cu(100) (55 cm^{-1})[74] and Cs/Ru(0001) (54–72 cm^{-1}).[75] When Cs was replaced with K, the frequency of the oscillating mode was 4.7 THz (157 cm^{-1}) at 0.32 ML, which agreed with that of the K–Pt stretching vibrational mode measured with HREELS.[76] Thus, these oscillating signals in TRSHG traces were attributed to coherent vibrations of the alkali atom–Pt stretching mode.

Resonant ISRS is a plausible excitation mechanism for the coherent oscillation of Cs and K. The problem is what type of electronic transition is involved in the excitation. The initial modulation amplitudes of TRSHG traces changed with alkali coverage, but did not mimic the variations in SH intensity. Namely, the oscillating signals were found only in the limited coverage range of 0.23–0.40 ML. This indicated that not all electronic resonance transitions that enhance second harmonic intensity are relevant to the creation of coherent vibration. Obviously, the electronic transition to create coherent vibration has to affect bonding nature of alkali-atoms with the metal substrate. Since the alkali layer in the coverage range cited above forms a metallic quantum well, the electronic states in the quantum well are primary candidates.

As described in Section **4.2**, there is an occupied alkali-induced state and a series of unoccupied image states in the

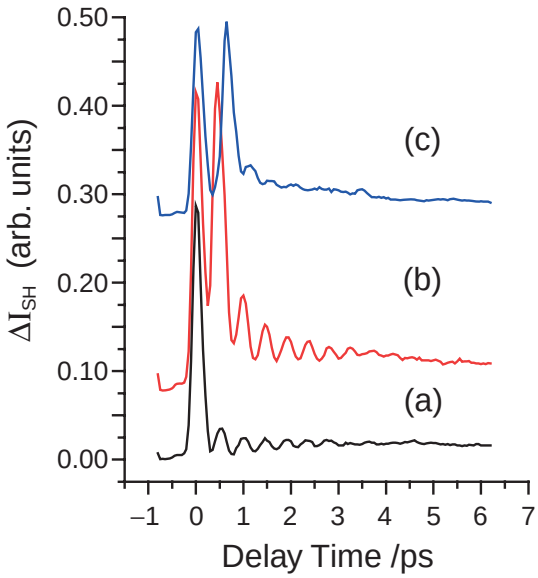

Fig. 13. TRSHG traces for Cs-covered Pt(111) surfaces with (a) single-pump-pulse excitation, (b) double-pump-pulse excitation in phase and (c) out-of-phase with respect to the oscillating signals due to the coherent Cs–Pt stretching vibration.

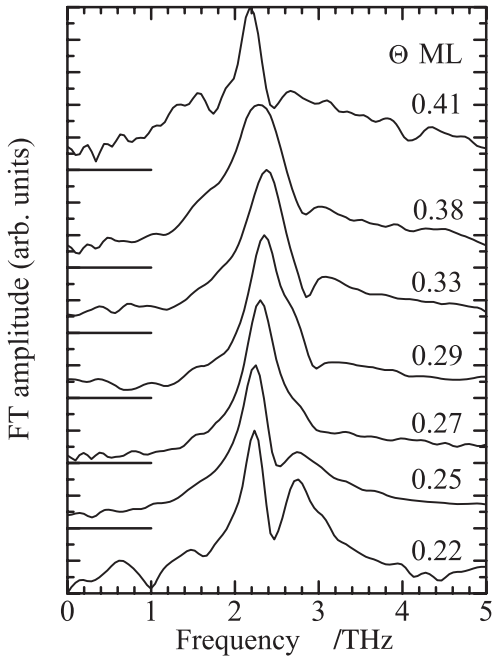

Fig. 14. Fourier amplitude spectra of the oscillatory parts of TRSHG signals for 800-nm pump at various Cs coverages. The spectra are normalized at their peaks. Reprinted with permission from Ref. 17. Copyright 2005, The American Physical Society.

metallic quantum well. The occupied alkali-induced state plays a central role in bonding of alkali atoms on the metal surfaces. Thus, creation of hole in the occupied state should be very effective to alter the deformation potentials for alkali atoms. One possible scenario is that the resonant transition from the occupied state to one of the image potential states effectively makes holes in the occupied state. In fact, recent TRSHG measurements on K/Pt(111) done in our laboratory as a function of excitation photon energy indicated that the oscillation amplitude in TRSHG traces increased when the photon energy was tuned to the resonance from the occupied state to the $j = 2$ image potential state. Since the alkali-induced occupied state has a large density in the vacuum side of the alkali layer as in the case of image potential states, the transition between the occupied to an image potential state has a large transition dipole moment. Although the resonant excitation between the surface-localized states is plausible, this is not the only mechanism for the creation of coherent vibration, since oscillating modulations due to the coherent stretching mode also appear even at the photon energy not resonant to the transition cited above.

Another possibility is that transitions in the bulk may contribute to creation of coherent phonons. For example, holes created in the d-bands due to the optical transitions in the bulk could be filled by electrons in the adsorbate-induced occupied state of the metallic quantum well as a result of an Auger-type transition. Since this Auger decay can occur significantly faster than the oscillation period of the alkali metal–Pt stretching mode, the substrate excitation may also be a possible excitation mechanism for the coherent oscillation.

In either case, a displacive force is exerted to alkali atom–Pt oscillators, leading to a cosine-like oscillation. In fact, the oscillating components observed in the TRSHG traces were all cosine-like. More detailed measurements of excitation photon energy dependence and calculations of the electronic structures of K and Cs/Pt(111) are needed for a clear understanding of the excitation mechanism.

4.4 Selective Excitation of a Surface Phonon Mode. Because of the wave-like nature of coherent oscillation, coherent surface phonons can interfere with each other. Figure 13 shows TRSHG traces with double pump pulses with approximately the same fluence instead of a single pump pulse. When the second pulse was fired at $t = 1.5T$ (Fig. 13c), where T is the oscillation period of the Cs–Pt stretching mode ($T = 435$ fs), the oscillation amplitude significantly decreased, i.e., destructive interference. On the contrary, when the second pulse was fired at $t = 1.0T$ (Fig. 13b), the oscillation amplitude nearly doubled, i.e., constructive interference. This wave-like nature of coherent phonons is used for selective excitation of a surface phonon mode as described later.

The coverage dependence of TRSHG traces was studied in detail for Cs/Pt(111).[17] Figure 14 shows the Fourier-transformed (FT) spectra of TRSHG traces as a function of Cs coverage. The FT spectral line was not symmetric and had a dip in the higher frequency side, indicating that at least two oscillating components with different initial phases contribute to the spectra. In fact, the TRSHG trace at 0.25 ML split into two frequency components of the main peak at 2.3 THz (77 cm^{-1}) of the Cs–Pt stretching mode and another peak at ≈2.8 THz (93 cm^{-1}) as shown in Fig. 15. The extra peak was assigned to the Pt surface Rayleigh phonon modes. Cs adsorbates form a (2 × 2) superstructure at $\theta = 0.26$ ML and a $(\sqrt{3} \times \sqrt{3})R30^\circ$ superstructure at $\theta = 0.33$ ML,[77] as in the case of K/Pt(111) described in Section **4.2**. As shown in Fig. 16, because of the adsorbate superstructures at the corresponding coverages, the Rayleigh modes at the surface Brillouin zone boundaries

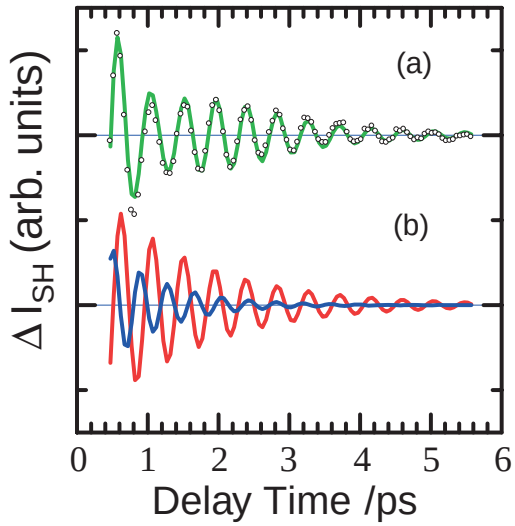

Fig. 15. (a) Fitting result of the TRSHG trace for the 0.25-ML Cs covered Pt(111) surface with two underdamped oscillating functions. (b) Two oscillating components with 2.3 and 2.8 THz obtained from the fitting. Note that the initial phases of the two components are different to each other.

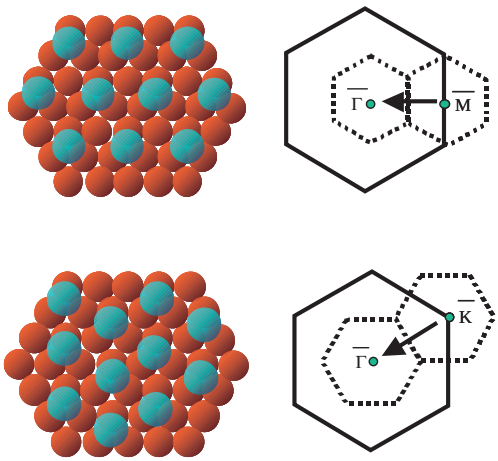

Fig. 16. Zone-boundary folding on Pt(111). The $\bar{M}$ and $\bar{K}$ points are folded back to the $\bar{\Gamma}$ point because of the superstructures of (a) p(2 × 2)-Cs and (b) ($\sqrt{3} \times \sqrt{3}$)-Cs, respectively.

of a clean platinum surface folded onto the $\bar{\Gamma}$ point so that they can be detected with TRSHG spectroscopy. In Section **4.3**, we stated that the formation of a hole in the alkali-induced state likely plays a major role for the excitation of the alkali-metal–Pt stretching mode. Although the wave function of this state is damped in the bulk, it can have finite amplitudes in a few Pt surface layers. Thus, the formation of a hole in this state can also excite the surface phonon modes coherently.

We demonstrated that a coherent mode can be selectively excited by using tailored fs-pulse trains.[78] The pulse trains were synthesized by using a pulse shaper consisting of a liquid-crystal spatial light modulator, a pair of gratings, and cylindrical lenses in a 4f configuration.[79] A periodic pattern of phase retardation with a period δF was implemented in the liquid-crystal array of the modulator that generates the pulse

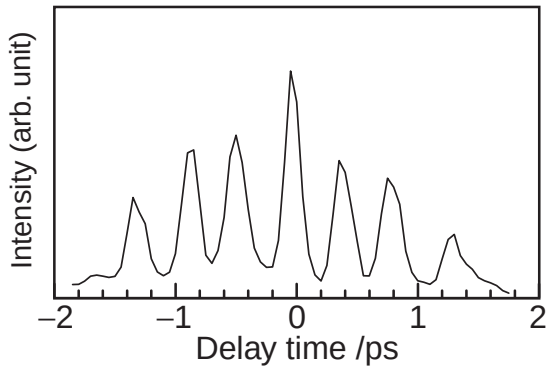

Fig. 17. Pulse train synthesized with a pulse shaper. The cross correlation trace was obtained between the pulse train and a 800-nm pulse with a pulse width of ≈130 fs. The period of the pulsed train can be varied from 2.0 to 2.9 THz.

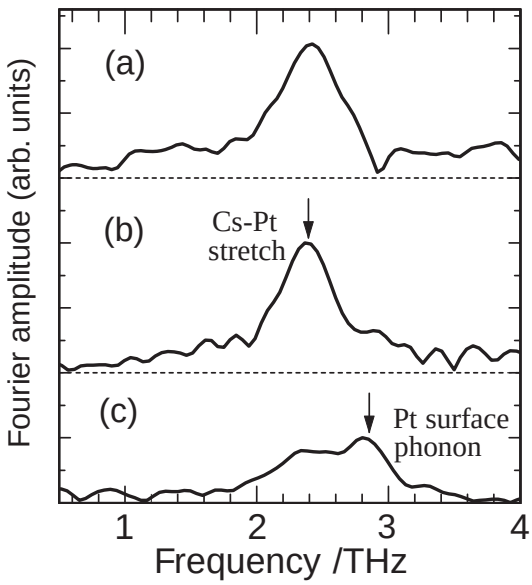

Fig. 18. Fourier amplitude spectra of TRSHG traces taken from 0.33-ML Cs-covered Pt(111) surfaces. (a) Obtained with single-pump-pulse configuration, (b) 7-pulse-pump configuration with a period of 2.3 THz, and (c) 7-pulse-pump configuration with a period of 2.9 THz. Enhancement in the amplitude of oscillation for a specific coherent mode takes place if the period of pulse train is matched to the frequency of a coherent phonon mode.

train with a period of $1/\delta F$. Binary phase-only filters, called Dammann gratings,[80,81] for the pulse-train generation produced flat-topped pulse trains with temporal cutoff edges. The filter pattern of the Dammann gratings for the number of pulses in a pulse train $N = 5$ or 7 were used according to the prescription given in Ref. 81. A typical example of a pulse train with $N = 7$ is shown in Fig. 17.

TRSHG traces were taken for 0.33-ML Cs covered Pt(111) excited with a pulse-train with $N = 7$ and the repetition rate was tuned from 2.0 to 2.9 THz. As shown in Fig. 18, for a pulse train with a 2.3-THz repetition rate, the Fourier spectrum of the TRSHG trace showed a strong peak at the same frequency as that of the pulse train envelope. However, as the

repetition rate was increased to 2.9 THz, the peak intensity at 2.3 THz decreased while that of the higher frequency component of the Rayleigh phonon mode increased.

The amplitude ratios between the Rayleigh mode and the Cs–Pt stretching mode obtained as a result of single pulse excitation were 0.72 and 0.25 at $\theta = 0.26$ and 0.33 ML, respectively. These ratios increased to 3.16 and 0.89 when a 2.9 THz pulse train was used. Thus, at both coverages, the ratios increased by a factor of $\approx$4. Consequently, these observations indicated that one can selectively excite either the Cs–Pt stretching mode or the Rayleigh phonon mode by tuning the repetition rate of the pulse train.

5. Conclusion

When we started studying the UV photochemistry of methane on Pt(111), there was little information on the interaction between methane and metal surfaces. In the last decade, theoretical and experimental studies have made a clearer picture of the interactions between alkanes and metal surfaces. In this account, we emphasized that the origin of the UV photochemistry is related to the longstanding problem of CH vibrational mode softening. To make this point more clearly, we need to pursue direct observations of hybridized states.

The active area in surface photochemistry has shifted from product analysis, including energy distributions of desorbed species, to monitoring nuclear dynamics in real time. TRSHG spectroscopy is very powerful for monitoring coherent vibrational motions of adsorbates and substrate atoms. We demonstrated this point in the studies on alkali-atom covered metal surfaces. Because the zone boundaries were folded back as a result of the formation of superstructures of alkali atoms, vibrational modes of adsorbates as well as surface phonon modes of the substrate could be observed by using TRSHG spectroscopy. Irradiation of a strong pump pulse creates highly nonequilibrium conditions between electron and lattice degrees of freedom. Thus, the observations of coherent surface phonons in the nonequilibrium conditions provided an interesting opportunity to examine electron–phonon coupling, which should be explored in more details in future.

Since coherent phonons have wave-like nature, they can interfer with each other. This interference was used to excite one of phonon modes selectively by using tailored fs laser pulse trains. Selective excitation of surface phonon modes is an important step toward a full understanding of surface reactions, since it is vital to know which phonon mode is most responsible for a chemical reaction to occur.

I wish to express my sincere appreciation to all of my research group members whose names are given in the references as co-authors. Particularly, I am very grateful for Kazuo Watanabe for the methane photochemistry and Kazuya Watanabe for the TRSHG studies. Without their dedication, the subjects described in this account would not have been realized. This work was supported in part by Grants-in-Aid for Scientific Research (S) (No. 17105001) from the Japan Society for the Promotion of Science (JSPS), and Scientific Research on Priority Area (417 Fundamental Science and Technology of Photofunctional Interfaces) from the Ministry of Education, Culture, Sports, Science and Technology (MEXT) of Japan.

References

1 T. J. Chuang, *Surf. Sci. Rep.* **1983**, *3*, 1.
2 X.-L. Zhou, X.-Y. Zhu, J. White, *Surf. Sci. Rep.* **1991**, *13*, 73.
3 W. Ho, *Surface Photochemistry*, World Scientific, **1995**, Chap. 24, pp. 1047–1140.
4 H. Petek, S. Ogawa, *Annu. Rev. Phys. Chem.* **2002**, *53*, 507.
5 C. Frischkorn, M. Wolf, *Chem. Rev.* **2006**, *106*, 4207.
6 Y. Matsumoto, K. Watanabe, *Chem. Rev.* **2006**, *106*, 4234.
7 D. Menzel, R. Gomer, *J. Chem. Phys.* **1964**, *41*, 3311.
8 P. A. Redhead, *Can. J. Phys.* **1964**, *42*, 886.
9 P. R. Antoniewics, *Phys. Rev. B: Condens. Matter Mater. Phys.* **1980**, *21*, 3811.
10 F. M. Zimmermann, W. Ho, *Surf. Sci. Rep.* **1995**, *22*, 127.
11 J. A. Misewich, T. F. Heinz, P. Weigand, A. Kalamarides, *Laser Spectroscopy and Photochemistry on Metal Surfaces*, ed. by H.-L. Dai, W. Ho, World Scientific Publishing, Singapore, **1995**, pp. 764–826.
12 M. Bonn, S. Funk, C. Hess, D. N. Denzler, C. Stempfl, M. Scheffler, M. Wolf, G. Ertl, *Science* **1999**, *285*, 1042.
13 D. N. Denzler, C. Frischkorn, C. Hess, M. Wolf, G. Ertl, *Phys. Rev. Lett.* **2003**, *91*, 226102.
14 H. Petek, M. J. Weida, H. Nagano, S. Ogawa, *Science* **2000**, *288*, 1402.
15 K. Watanabe, N. Takagi, Y. Matsumoto, *Chem. Phys. Lett.* **2002**, *366*, 606.
16 K. Watanabe, N. Takagi, Y. Matsumoto, *Phys. Rev. Lett.* **2004**, *92*, 57401.
17 K. Watanabe, N. Takagi, Y. Matsumoto, *Phys. Rev. B* **2005**, *71*, 85414.
18 L. C. Lee, C. C. Chiang, *J. Chem. Phys.* **1983**, *78*, 688.
19 Y. A. Gruzdkov, K. Watanabe, K. Sawabe, Y. Matsumoto, *Chem. Phys. Lett.* **1994**, *227*, 243.
20 K. Watanabe, M. Lin, Y. A. Gruzdkov, Y. Matsumoto, *J. Chem. Phys.* **1996**, *104*, 5974.
21 Y. Matsumoto, Y. Gruzdkov, K. Watanabe, K. Sawabe, *J. Chem. Phys.* **1996**, *105*, 4775.
22 Y. A. Gruzdkov, K. Watanabe, K. Sawabe, Y. Matsumoto, *Surf. Sci.* **1996**, *363*, 195.
23 K. Watanabe, K. Sawabe, Y. Matsumoto, *Phys. Rev. Lett.* **1996**, *76*, 1751.
24 K. Watanabe, Y. Matsumoto, *Surf. Sci.* **2000**, *454–456*, 262.
25 J. E. Demuth, H. Ibach, S. Lehwald, *Phys. Rev. Lett.* **1978**, *40*, 1044.
26 M. A. Chesters, S. F. Parker, R. Raval, *J. Electron Spectrosc. Relat. Phenom.* **1986**, *39*, 155.
27 R. Raval, M. A. Chesters, *Surf. Sci. Lett.* **1989**, *219*, L505.
28 R. Raval, S. F. Parker, M. A. Chesters, *Surf. Sci.* **1993**, *289*, 227.
29 G. Witte, K. Weiss, P. Jakob, J. Braun, K. L. Kostov, C. Wöll, *Phys. Rev. Lett.* **1998**, *80*, 121.
30 K. Weiss, J. Weckesser, C. Wöll, *THEOCHEM* **1999**, *458*, 143.
31 C. Wöll, *J. Synchrotron Rad.* **2001**, *8*, 129.
32 C. Wöll, K. Weiss, P. Bagus, *Chem. Phys. Lett.* **2000**, *332*, 553.
33 K. A. Fosser, R. G. Nuzzo, P. S. Bagus, C. Wöll, *Angew. Chem., Int. Ed.* **2002**, *41*, 1735.

34 K. A. Fosser, R. G. Nuzzo, P. S. Bagus, C. Wöll, *J. Chem. Phys.* **2003**, *118*, 5115.
35 M. B. Robin, *Higher Excited States of Polyatomic Molecules*, Academic Press, Inc., Orlando, **1985**, Vol. 3.
36 B. H. Mahan, R. Mandal, *J. Chem. Phys.* **1962**, *37*, 207.
37 T. G. Slanger, G. Black, *J. Chem. Phys.* **1982**, *77*, 2432.
38 J.-H. Wang, K. Liu, *J. Chem. Phys.* **1998**, *109*, 7105.
39 J.-H. Wang, K. Liu, Z. Min, H. Su, R. Bersohn, J. Preses, J. Z. Larese, *J. Chem. Phys.* **2000**, *113*, 4146.
40 S. Karplus, R. Bersohn, *J. Chem. Phys.* **1969**, *51*, 2040.
41 M. S. Gordon, J. W. Caldwell, *J. Chem. Phys.* **1979**, *70*, 5503.
42 A. M. Mebel, S.-H. Lin, C.-H. Chang, *J. Chem. Phys.* **1997**, *106*, 2612.
43 J. Yoshinobu, H. Ogasawara, M. Kawai, *Phys. Rev. Lett.* **1995**, *75*, 2176.
44 F. Zaera, H. Hoffmann, *J. Phys. Chem.* **1991**, *95*, 6297.
45 D. W. Fairbrother, X. D. Peng, R. Viswanathan, P. C. Stair, M. Trenary, J. Fan, *Surf. Sci.* **1993**, *285*, L435.
46 V. A. Ukraintsev, I. Harrison, *Surf. Sci. Lett.* **1993**, *286*, L571.
47 D. Yamaguchi, T. Matsumoto, K. Watanabe, N. Takagi, Y. Matsumoto, *Phys. Chem. Chem. Phys.* **2006**, *8*, 179.
48 Y. Akinaga, T. Taketsugu, K. Hirao, *J. Chem. Phys.* **1997**, *107*, 415.
49 Y. Akinaga, T. Taketsugu, K. Hirao, *J. Chem. Phys.* **1998**, *109*, 11010.
50 H. Öström, L. Triguero, M. Nyberg, H. Ogasawara, L. G. M. Pettersson, A. Nilsson, *Phys. Rev. Lett.* **2003**, *91*, 046102.
51 H. Öström, L. Triguero, K. Weiss, H. Ogasawara, M. G. Garnier, D. Nordlund, M. Nyberg, L. G. M. Pettersson, A. Nilsson, *J. Chem. Phys.* **2003**, *118*, 3782.
52 H. Öström, H. Ogasawara, L.-Å. Näslund, L. G. M. Pettersson, A. Nilsson, *Phys. Rev. Lett.* **2006**, *96*, 146104.
53 Y. R. Shen, *The Principles of Nonlinear Optics*, John Wiley, New Jersey, **2003**.
54 S. Mukamel, *Principles of Nonlinear Optical Spectroscopy*, Oxford Univ. Press, New York, **1995**.
55 L. Dhar, J. A. Rogers, K. A. Nelson, *Chem. Rev.* **1994**, *94*, 157.
56 H. J. Zeiger, J. Vidal, T. K. Cheng, E. P. Ippen, G. Dresselhaus, M. S. Dresselhaus, *Phys. Rev. B* **1992**, *45*, 768.
57 A. V. Kuznetsov, C. J. Stanton, *Phys. Rev. Lett.* **1994**, *73*, 3243.
58 T. Dekorsy, G. C. Cho, H. Kurz, *Coherent Phonons in Condensed Media* in *Topics in Applied Physiscs*, Springer Verlag, Berlin Heidelberg, **2000**, Vol. 76, pp. 169–209.
59 O. V. Misochko, M. Hase, M. Kitajima, *Phys. Solid State* **2004**, *46*, 1741.
60 H. P. Bonzel, *Surf. Sci. Rep.* **1988**, *8*, 43.
61 T. Aruga, Y. Murata, *Prog. Surf. Sci.* **1989**, *31*, 61.
62 C. T. Campbell, *Annu. Rev. Phys. Chem.* **1990**, *41*, 775.
63 A. G. Naumovets, *Surf. Sci.* **1994**, *299–300*, 706.
64 R. D. Diehl, R. McGrath, *Surf. Sci. Rep.* **1996**, *23*, 43.
65 G. Pirug, H. P. Bonzel, *Surf. Sci.* **1988**, *194*, 159.
66 R. W. Gurney, *Phys. Rev.* **1935**, *47*, 479.
67 N. Fischer, S. Schuppler, R. Fischer, T. Fauster, W. Steinmann, *Phys. Rev. B* **1991**, *43*, 14722.
68 N. Fischer, S. Schuppler, T. Fauster, W. Steinmann, *Surf. Sci.* **1994**, *314*, 89.
69 D. Tang, D. McIlroy, X. Shi, D. Heskett, *Surf. Sci. Lett.* **1991**, *255*, L497.
70 J. M. Carlsson, B. Hellsing, *Phys. Rev. B* **2000**, *61*, 13973.
71 G. Hoffmann, J. Kliewer, R. Berndt, *Phys. Rev. Lett.* **2001**, *87*, 176803.
72 S. Å. Lindgren, L. Walldén, *Phys. Rev. B* **1992**, *45*, 6345.
73 K. J. Song, D. Heskett, H. L. Dai, A. Liebsch, E. W. Plummer, *Phys. Rev. Lett.* **1988**, *61*, 1380.
74 G. Witte, J. P. Toennies, *Phys. Rev. B* **2000**, *62*, R7771.
75 P. He, Y. Xu, K. Jacobi, *J. Chem. Phys.* **1996**, *104*, 8118.
76 C. Klünker, C. Steimer, J. B. Hannon, M. Giesen, H. Ibach, *Surf. Sci.* **1999**, *420*, 25.
77 J. Cousty, R. Riwan, *Surf. Sci.* **1988**, *204*, 45.
78 K. Watanabe, N. Takagi, Y. Matsumoto, *Phys. Chem. Chem. Phys.* **2005**, *7*, 2697.
79 M. M. Wefers, K. A. Nelson, *J. Opt. Soc. Am. B* **1995**, *12*, 1343.
80 A. M. Weiner, D. E. Leaird, *Opt. Lett.* **1990**, *15*, 51.
81 U. Killat, G. Rabe, W. Rave, *Fiber Integr. Opt.* **1982**, *4*, 159.
82 J. Schirmer, A. B. Trofimov, K. J. Randall, J. Feldhaus, A. M. Bradshaw, Y. Ma, C. T. Chen, F. Sette, *Phys. Rev. A* **1993**, *47*, 1136.

Yoshiyasu Matsumoto was born and raised in Kyoto, Japan. He received his Bachelor and Master degrees in industrial chemistry from Kyoto University and his Doctor degree in reaction chemistry from the University of Tokyo in 1981. Following appointments as a postdoctoral researcher in the University of Pittsburgh working with Professor David W. Pratt and a research scientist at RIKEN institute working with Dr. M. Takami, he was appointed as an Associate Professor at Institute for Molecular Science (IMS) in 1990. He moved to the Graduate University for Advanced Studies (SOKENDAI) as a full Professor in 1997, and has been a Professor at IMS since 2004 with a joint appointment in SOKENDAI. He received the Award for Creative Work from the Chemical Society of Japan in 2006. His current research interests include photo-induced dynamics and reactions at surfaces and interfaces, catalytic reactions, and the electronic structure and reactivity of nano-structured materials.